JOURNAL OF MATERIALS SCIENCE **40** (2005) 4737–4748

Studies on the ionic transport and structural investigations of $La_{0.5}Li_{0.5}TiO_3$ perovskite synthesized by wet chemical methods and the effect of Ce, Zr substitution at Ti site

HRUDANANDA JENA*, K. V. GOVINDAN KUTTY
Materials Chemistry Division, Indira Gandhi Centre for Atomic Research, Kalpakkam-603 102, India
E-mail: hnje@igcar.ernet.in

T. R. N. KUTTY
Materials Research Centre, Indian Institute of Science, Bangalore-560012, India

Published online: 08 July 2005

$La_{0.5}Li_{0.5}TiO_3$ perovskite was synthesized by various wet chemical methods. By adopting low temperature methods of preparation lithium loss from the material is prevented. $La_{0.5}Li_{0.5}TiO_3$ (LLTO) was formed with cubic symmetry at 1473 K. LLTO was formed at relatively lower temperature by using hydrothermal preparation method. PVA gel-decomposition route yield tetragonal LLTO on annealing the dried gel at 1473 K. By using gel-carbonate route $LiTi_2O_4$ minor phase was found to remain even after heat-treatment at 1473 K. The hydroxylation of LLTO was done in deionized water as well as in dilute acetic acid medium. By hydroxylation process incorporation of hydroxyls and leaching out of Li^+ was observed from the material. The Li^+ concentration of these compositions was examined by AAS. The electrical conductivities of these compositions were measured by dc and ac impedance techniques at elevated temperatures. The activation energies of electrical conduction for these compositions were estimated from the experimental results. The measured activation energy of Li^+ conduction is 0.34 eV. Unhydroxylated samples exhibit only Li^+ conduction, whereas, the hydroxylated LLTO show proton conductivity at 298–550 K in addition to Li^+ conductivity. The effect of Zr or Ce substitution in place of Ti were attempted. $La_{0.5}Li_{0.5}ZrO_3$ Perovskite was not formed; instead pyrochlore phase ($La_2Zr_2O_7$) along with monoclinic ZrO_2 phases was observed above 1173 K; below 1173 K cubic ZrO_2 is stable. $(La_{0.5}Li_{0.5})_2CeO_4$ solid solution was formed in the case of Ce substitution at Ti sublattice on heat-treatment up to 1673 K.

1. Introduction

A wide variety of inorganic solids are known to exhibit high lithium ion conductivity. The well-known materials are (i) lithium oxyacid salts [1, 2] (ii) LISICON [3] (iii) NASICON structured $Li_{1+x}Ti_{2-x}M_x(PO_4)_3$ (M = Al, Ga, In, Sc) [4] and (iv) A-site deficient perovskite solid solutions. The highest bulk lithium ion-conducting solid electrolyte is the perovskite (ABO_3)–type, lithium lanthanum titanate ($Li_{3x}La_{(2/3)-x}V_{(1/3)-2x}TiO_3$ ($0.04 < x < 0.16$ and V = vacancy)) and materials with the related structure [5–12], which may be abbreviated as LLTO for convenient use. The lithium ion conducting perovskite oxides show high ionic conductivity in the range of 10^{-5}–10^{-3} S/cm [5–12] at room temperature and are stable at high temperatures, so that they are promising materials for various applications such as high energy batteries, Li-ion separators and other electrochemical devices. Lithium ion conductivity in $Li_{3x}La_{(2/3)-x}V_{(1/3)-2x}TiO_3$ (V = vacancy) originates from the diffusion of lithium ions via vacancies among A-sites. The selective permitivity of $Li_{3x}La_{(2/3)-x}V_{(1/3)-2x}TiO_3$ (V = vacancy) to Li^+ ion diffusion can be utilized to separate Li^+ from other alkali metal ions as well as to separate ^6Li from ^7Li isotope by using the perovskite (as separator) on electrolysis [13].

The crystal structure of LLTO perovskite was studied by various investigators; a simple cubic perovskite

*Author to whom all correspondence should be addressed.
0022–2461
DOI: 10.1007/s10853-005-0480-7

structure was first claimed for $La_{0.5}Li_{0.5}TiO_3$ [14, 15], while other studies proposed an orthorhombic structure [16] or a tetragonal tungsten bronze structure [17]. Many studies reported in literature emphasized on the structure and properties of $Li_{3x}La_{(2/3)-x}V_{(1/3)-2x}TiO_3$ (V = vacancy) phases [12, 18–20] especially to understand the mechanism of Li^+ ion conduction, which essentially involves the A sites that contain a combination of La, Li and vacancies. A number of structural polymorphs occur for this phase as a function of both temperature and composition [21]. The compositions of LLTO studied and reported in the literature were mostly prepared by solid-state reaction route. The solid-state reaction route involves repeated grinding and soaking of reactant powders at temperatures between 1500–1600 K for several hours (10–15 h). The annealing of these powders at high temperatures leads to loss of lithium as Li_2O, thereby decreasing the concentration of Li^+ (current carriers), and a decrease in conductivity of the material. This can be avoided by adopting suitable low temperature methods of synthesis. Kitaoka *et al.* [22] reported the preparation of $La_{0.5}Li_{0.5}TiO_3$ thin films by sol-gel route by using metal acetates and Ti-isopropoxides as starting materials. Preparation of $Li_{3x}La_{(2/3)-x}V_{(1/3)-2x}TiO_3$ (V = vacancy) compositions by using other wet chemical routes such as metal hydroxide-poly vinyl alcohol (PVA) gel decomposition method and hydrothermal processing routes using easily available starting materials, are rarely reported in the literature. In this study, such methods are employed. The compositions were also prepared by using hydroxide or carbonate precipitates of lanthanum, $TiO_2 \cdot xH_2O$ and $LiOH \cdot H_2O$ as starting materials and their properties are studied and compared with products obatined from PVA-gel decomposition and hydrothermal routes. The samples prepared were subjected to hydrothermal leaching of Li^+ and incorporation of hydroxyls in to the lattice. The hydrogen/ deuterium exchange experiment was also carried out to confirm hydrogen exchange, which may give rise to proton mobility (H_3O^+) in these solids. Preparation of $Li_{3x}La_{(2/3)-x(1/3)-2x}MO_3$ (M = Zr, Ce and = vacancy) by replacing Ti^{4+} with Zr^{4+} and Ce^{4+} were also attempted. The materials were characterized by various techniques and the electrical transport properties of these compositions were measured by AC and DC techniques in the temperature range of 298–1273 K. The results obtained in these experiments are presented in this paper.

2. Experimental

2.1. Sample preparation

2.1.1. Preparation of $La_{1-x}Li_xMO_3$, ($M = Zr, Ti$ and Ce, $x = 0.5$) by hydrothermal route

Stoichiometric amounts of $TiO_2 \cdot xH_2O$ ($3 < x < 8$) gels were precipitated from $TiOCl_2$ solution by adding NH_4OH and the gels were washed free from chloride [23, 24]. Stoichiometric amounts of La_2O_3 (M/s. Indian Rare Earths Ltd. India) was dissolved in HNO_3 and precipitated as $La(OH)_3$, filtered and mixed with the TiO_2 gel. The entire mixture was put in a teflon beaker with lid and heated at 423 K under hydrothermal condition for 4 h. The reaction product was taken out of the hydrothermal vessel after cooling to room temperature and filtered. Stoichiometric amounts of $Li(OH) \cdot H_2O$(M/s. Loba Chemie Pvt. Ltd, India) was mounted on to the hydrothermally prepared product and dried. The thoroughly mixed slurry-like precursor was calcined at 1173 K for 5 h and subsequently at 1473 K for 4 h. Similarly, the preparation of $La_{0.5}Li_{0.5}ZrO_3$ and $La_{0.5}Li_{0.5}CeO_3$ were attempted by using $ZrO_2 \cdot xH_2O$ and $CeO_2 \cdot xH_2O$ precipitated from $ZrOCl_2 \cdot 8H_2O$ (M/s. K.Chem. India) and $Ce^{4+}(NH_4)_2(NO_3)_6$ (M/s. Sarabhai M.Chemicals, India) salts respectively. The products obtained were characterized by XRD and other techniques.

2.1.2. Preparation of $La_{1-x}Li_xMO_3$, ($M = Zr, Ti$ and Ce, $x = 0.5$) carbonate co- precipitation route (gel-carbonate route)

Stoichiometric amounts of TiO_2 and $La(NO_3)_3$ as described above (Section 2.1.1) were taken along with $Li(OH) \cdot (NH_4)_2CO_3$ solution was added to the mixed solution of $La(NO_3)_3$ and $LiOH \cdot H_2O$ and carbonates of La and Li were co-precipitated. The precipitate (submicron particles of the carbonates) was filtered and dispersed in the voluminous titania gel ($TiO_2 \cdot xH_2O$). The slurry ($TiO_2 \cdot xH_2O$ + carbonates of La and Li) was oven dried and the powders were calcined at 1173 K for 4 h. This procedure was repeated to prepare Zr and Ce analogues by using $ZrO_2 \cdot xH_2O$ and $CeO_2 \cdot xH_2O$ instead of $TiO_2 \cdot xH_2O$ gel and the products were characterized.

2.1.3. Preparation of $La_{0.5}Li_{0.5}TiO_3$ by decomposition of metal-polyvinyl alcohol (PVA) gel

Stoichiometric concentrations of $TiO_2 \cdot xH_2O$ and $La(NO_3)_3$ as described in Section 2.1.1 were taken along with $Li(OH) \cdot H_2O$. Poly Vinyl Alcohol (-[-CH_2-CHOH-]-$_n$) was taken 3-times the molar ratio of the reactants and added to the mixture of reactants. The reaction mixture was sonicated for 30 min. in an ultrasonic cleaner for homogenization. The homogeneous mixture was heated on a hot plate at 400 K for 1 h. The solution dried up and charred to a fluffy mass. The fluffy mass was subsequently calcined at 1173 K or higher temperatures to obtain the single-phase perovskite in lanthanum lithium titanium oxide system.

2.2. Experimental methods of characterization

The oven-dried powders were examined by X-ray powder diffraction employing a Siemens D-500 powder X-ray diffractometer in the step-scan mode with a step size of 0.02 deg. $2\theta/s$ with a counting time of 5 s per step using Cu K_α radiation. XRD patterns of the powders were indexed by using STADIP and X'pert Plus software. The powders were also examined by TG/DTA (STA-1500, Rheometric Scientific, U.K) in order to find out the weight loss characteristics as well as phase transformation within the programmed temperature range.

The infra-red (IR) spectra of the phase-pure powders were taken in KBr as well as KCl matrix to identify the presence of O–H groups (Bomem, MB-100 FTIR, resolution 4 cm^{-1}).

The powders sintered at 1523 K for 4 h were subjected to hydrothermal treatment in a teflon vessel with lid, the purpose of doing this experiment was to investigate the possibility of ion exchange of Li^+ with proton. Experiments were carried out in D_2O medium as well as D_2O containing weak organic acids (10% *v/v* acetic acid). The leachant solution was analysed for Li, Ti and La by Atomic Absorption Spectroscopy (AAS). Li^+ was found to leach out of the material. The Li^+ leached out concentration was twice in weak organic acid compared to ordinary deionized water medium. The pellet surface was examined by Scanning Electron Microscope (SEM XL 30, Philips) and the particle size of the material was measured before and after sintering.

2.3. Electrical conductivity measurement

Electrical conductivity of the samples was measured by DC as well as AC methods in air. The details of the cell arrangement and sample mounting in the cell are discussed in earlier papers [24–26]. The cylindrical pellets of 5 mm diameter and 8 mm length were used to measure the electrical conductivity in the temperature range of 298–1273 K. The total conductivity of the specimens was measured by the DC method. Ag or Pt electrodes were used to measure the electrical resistivity of the rod-shaped samples. A Solartron-1255 frequency response analyser backed by a Solartron 1286 electrochemical interface was employed for AC measurements. The frequency range covered in a typical experiment was 1Hz to 10 MHz.

3. Results and discussion

3.1. Effect of preparation conditions and temperature on the phase stability of $La_{0.5}Li_{0.5}TiO_3$, compositions

These perovskites ($Li_{3x}La_{(2/3)-x}V_{(1/3)-2x}TiO_3$ ($0.06 < x < 0.16$ and V = vacancy)) exhibit various crystal structures, depending on the preparation conditions (temperature, annealing ambient etc.) and the nature of substituents. $La_{0.5}Li_{0.5}TiO_3$ stabilizes in perovskite phase. A cubic structure is obtained by adopting hydrothermal treatment of $TiO_2{\cdot}xH_2O$ gel with $La(OH)_3$ and then mounting $LiOH{\cdot}H_2O$ to the hydrothermal reaction product. The latter mixture on annealing at 1473 K for 4 h produces single phase, $La_{0.5}Li_{0.5}TiO_3$. The XRD pattern of the composition is given in Fig. 1a. The powders prepared by hydrothermal treatment of $La(OH)_3{\cdot}xH_2O + TiO_2{\cdot}xH_2O$ gel and subsequent addition of $LiOH{\cdot}H_2O$ gave a slurry; the slurry was oven dried and subsequently annealed in a Pt boat at 1100–1273 K for 4 h to yield cubic perovskite phase. The lattice parameters calculated by using X'pert pro package for this composition is given in Table I. In this preparation method loss of Li was more from the compound that was confirmed by the AAS examination of the product. In this case the powders were observed to react with the Pt boat forming a grey black coloured stain on the Pt surface after annealing.

The product obtained from PVA gel decomposition produces a tetragonal phase (Figs 1b and 2). The chemical reaction can be written as follows

$$2TiO_2{\cdot}xH_2O\,(\text{gel}) + La(OH)_3\,(\text{precipitate}) + LiOH{\cdot}H_2O + 2\,\text{wt\% PVA} \xrightarrow{1100\ \text{K(calcined)}} 2\,La_{0.5}Li_{0.5}TiO_3 + CO_2(g) + xH_2O\,(\text{vapour}) \quad (1)$$

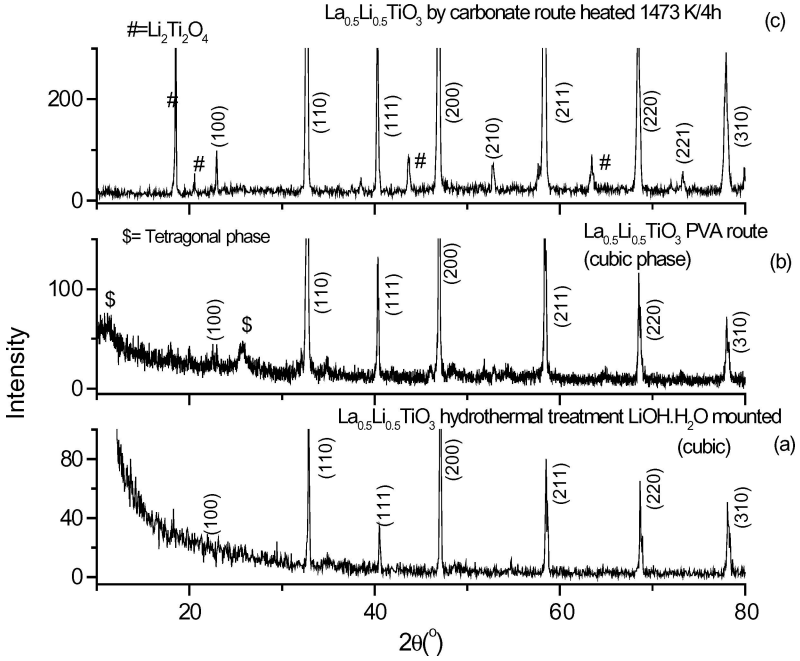

Figure 1 XRD patterns of $La_{0.5}Li_{0.5}TiO_3$ prepared by various routes, heated at 1473 K/ 6 h (a) hydrothermal precursor route (b) PVA gel decomposition route(c) carbonateprecipitation route.

TABLE I Lattice parameters and densities determined at 298 K after sintering the compositions at indicated temperatures

Compositions/Preparation route	Sintering temperature (K)/4 h	Lattice constants (Å) (XRD at 298 K)	Density in (g/cm^3)
$La_{0.5}Li_{0.5}TiO_3$			
(i) hydroxide + pva route	1173 K /4 h	Tetragonal, S.G : P4/mmm	4.999 [31]
	1273 K/4 h	$a = 3.873(1)$	3.431(2)
	1473 K/4 h	$c = 7.787(1)$	3.898(2)
	1523 K /4 h	-do-	4.023(1)
(ii) hydrothermally	1473 K /5 h	(ii) Cubic, S.G.: Pm3m	4.005(1)
treated ($La(OH)_3 + TiO_2$)		$a = 3.854(1)$	
$LiOH.H_2O$			
(iii) Carbonate	1273 K/4 h	(iii) $a = 3.854(2)$ Pm3m with	
precipitation route		impurity phases $Li_2Ti_2O_4$	
*($La_{0.5}Li_{0.5}$) CeO_3)		$a = 5.412(1)$ for CeO_2, S.G	7.211(1) for
		:Fm3m [31]	CeO_2 [31]
(i) hydroxide+PVA route	1273 K/4 h	$a = 5.465(1)$, solid solution	–
	1473 K/4 h	$a = 5.508(1)$	
	1673 K/4 h	$a = 5.509(1)$	
*($La_{0.5}Li_{0.5}$) ZrO_3		$a = 5.152(2)$ ZrO_2, S.G:	5.883 (1) for
(i) hydroxide+PVA route		Fm3m[31].	ZrO_2), [31]
above 1023 K formation	1023 K/4 h	$a = 5.302(1)$. (Solid solution),	
of pyrochlore ($La_2Zr_2O_7$)	above 1123 K	$a = 10.780(1)$,S.G=Fd3m	6.068 (2)[31]
+ monoclinic ZrO_2		$a = .313(1)$,$b = 5.211(1)$	5.817 (1)[31]
		$c = 5.146(1)$, S.G=$P2_1/a$	

*Nominal composition attempted, in reality it form solid solution $(La_{0.5}Li_{0.5})_2MO_4$, (M=Ce or Zr).

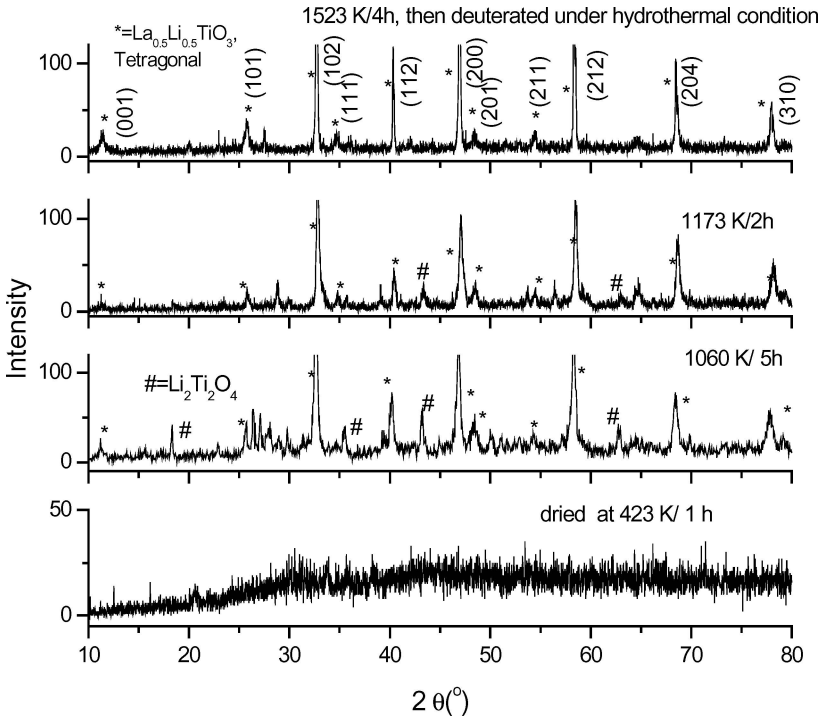

Figure 2 XRD patterns of $La_{0.5}Li_{0.5}TiO_3$ prepared by PVA gel decomposition route and annealed at indicated temperatures.

The TGA/DTA plot of the powders is shown in Fig. 3. The total weight loss was ∼18%. The endotherm at ∼380–400 K corresponds to the H_2O loss (13%). The endotherm at 750 K corresponds to the loss of hydroxyls. The exotherm at 1060 K is a recrystallization step leading to the formation of perovskite phase. The powders annealed at 1060–1100 K show evolution of $La_{0.5}Li_{0.5}TiO_3$ as the major phase in XRD examinations. The temperature of phase formation was thus examined by TG/DTA and XRD studies.

The powders obtained from carbonate decomposition route contain $Li_2Ti_2O_4$ as a minor phase at 1060 K (Fig. 1c). $Li_2Ti_2O_4$ phase was found to vanish on annealing the powders above 1573 K. The powders prepared by carbonate co-precipitation and PVA gel decomposition route did not show stains on the Pt boat surface after annealing above 1173 K. The presence of $Li_2Ti_2O_4$ in the product obtained from carbonate precipitation route (Fig. 1c) below 1473 K is observed.

The effect of hydroxyls on crystal structure and other properties were studied by subjecting the powders to ion exchange of Li^+ with H^+ or deuterium ions. The experiments carried out in deionized H_2O + D_2O medium under hydrothermal conditions did not yield any remarkable results. However, the experiments carried out in weak organic acid (acetic

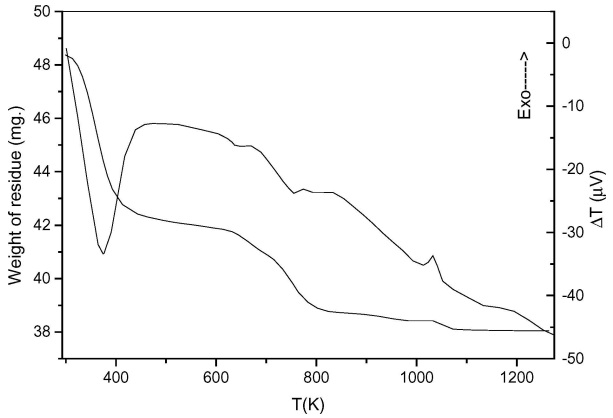

Figure 3 TG/DTA plot of $La_{0.5}Li_{0.5}TiO_3$ prepared by hydroxide co-precipitation and PVA added gel dried at 400 K, TG/DTA carried out on dried gel.

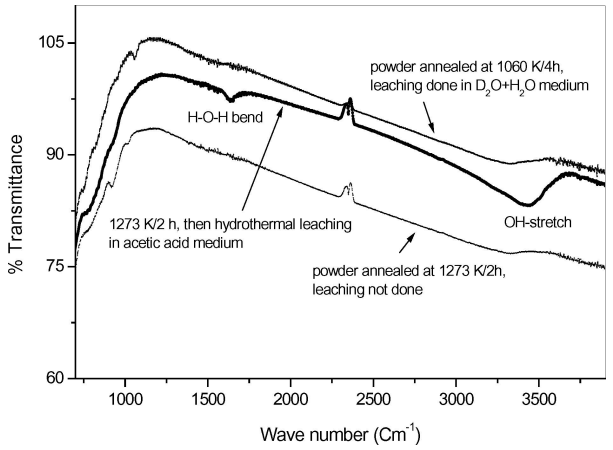

Figure 4 IR spectra of $La_{0.5}Li_{0.5}TiO_3$ annealed at the temperatures indicated and then treated under hydrothermal conditions to incorporate hydroxyls from $H_2O + D_2O$ and $H_2O + D_2O$ + acetic acid medium.

acid) medium under hydrothermal condition showed incorporation of hydroxyls into the crystal lattice. In both the cases leaching out of Li^+ was observed. The leaching of Li^+ in acetic acid medium is faster and more complete when compared to that in neutral (pH = 7) medium. The incorporation of OH groups to the lattice was confirmed by FTIR examination of the powders after the leaching studies. The IR absorption band at 3450 cm^{-1} is assigned to O–H stretch and at 1640 cm^{-1} is attributed to H–O–H bending for the sample processed in acetic acid medium (Fig. 4). The IR absorption band, in the case of samples treated in deionized water at 3350 cm^{-1} are very weak; this may be due to the presence of very small amounts of hydroxyls and possibly were not significant. The XRD patterns and hence the crystal structure of the compounds were not changed after leaching out of Li^+ under these experimental conditions.

The crystal structure of $La_{0.5}Li_{0.5}TiO_3$ is drawn by using Diamond Software taking experimentally measured lattice parameters (Table I) as the input data and the structure is given in Fig. 5a. The experimentally measured lattice parameters agree well with the reported values for the compositions $Li_{3x}La_{(2/3)-x}V_{(1/3)-2x}TiO_3 (x \cong 0.09 - 0.13$ and V = vacancy) [27]. The stabilization of cubic structure (S.G = Pm3m) may be attributed to the random distribution of La^{3+}, Li^+ ions and vacancies over the A-sites. The tetragonal structure obtained in case of PVA gel decomposition route on annealing at 1523 K is drawn using the experimentally measured lattice parameters is given in Fig. 5b. The tetragonal distortion was attributed to the unequal distribution of vacancies, Li^+ and La^{3+} cations on the two possible crystallographic sites 1a and 1b (12-fold coordination with

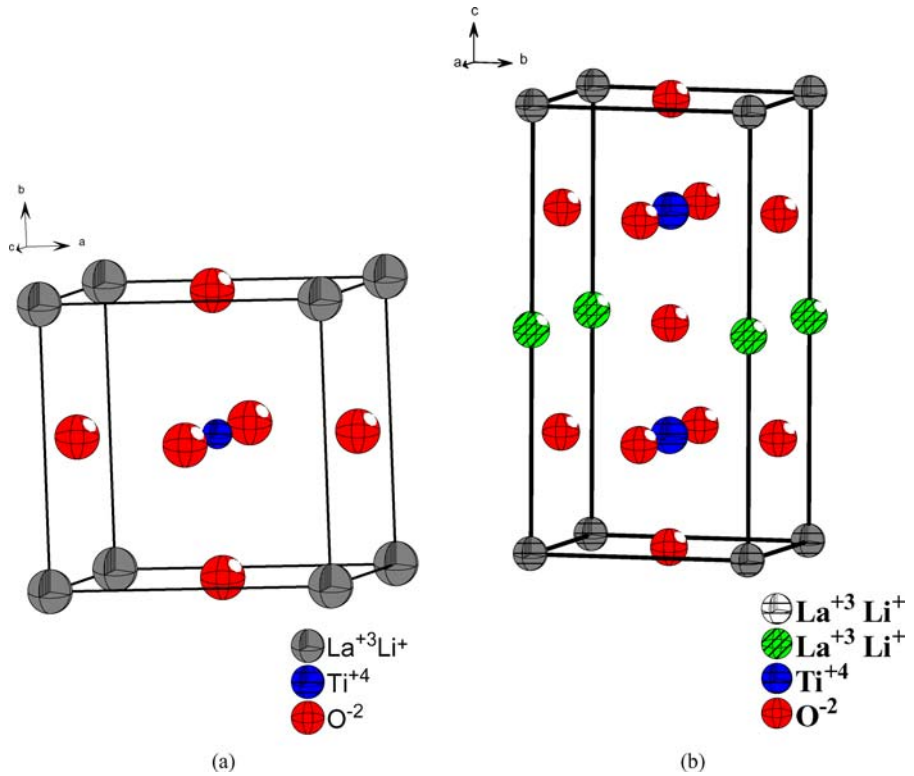

Figure 5 Crystal structure of $La_{0.5}Li_{0.5}TiO_3$ (a) Cubic, (a = 3.873Å) (b) Tetragonal, (a = 3.873 c = 7.787 Å).

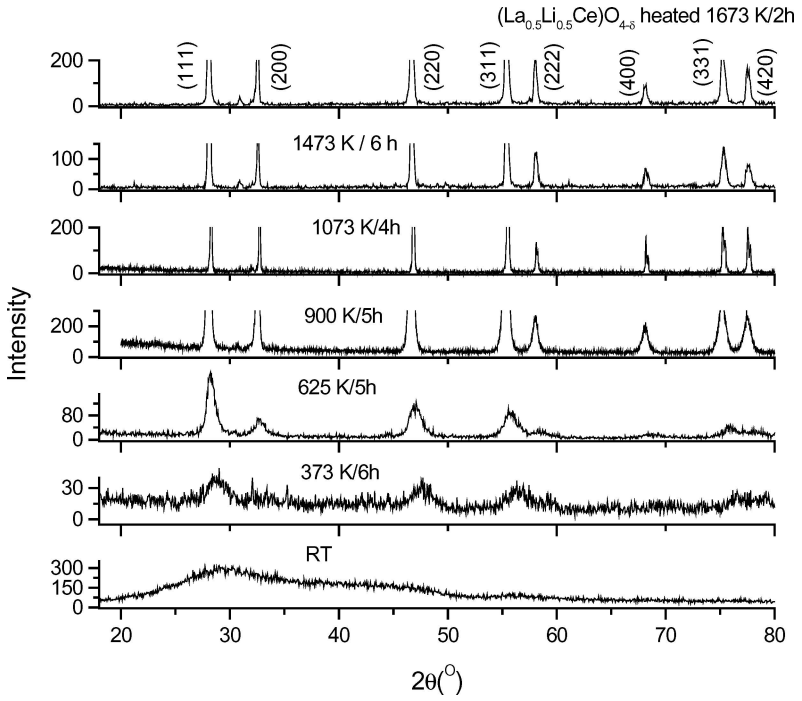

Figure 6 XRD patterns of $((La_{0.5}Li_{0.5})_2Ce)O_4$ annealed at indicated temperatures, solid solutions of cubic CeO_2.

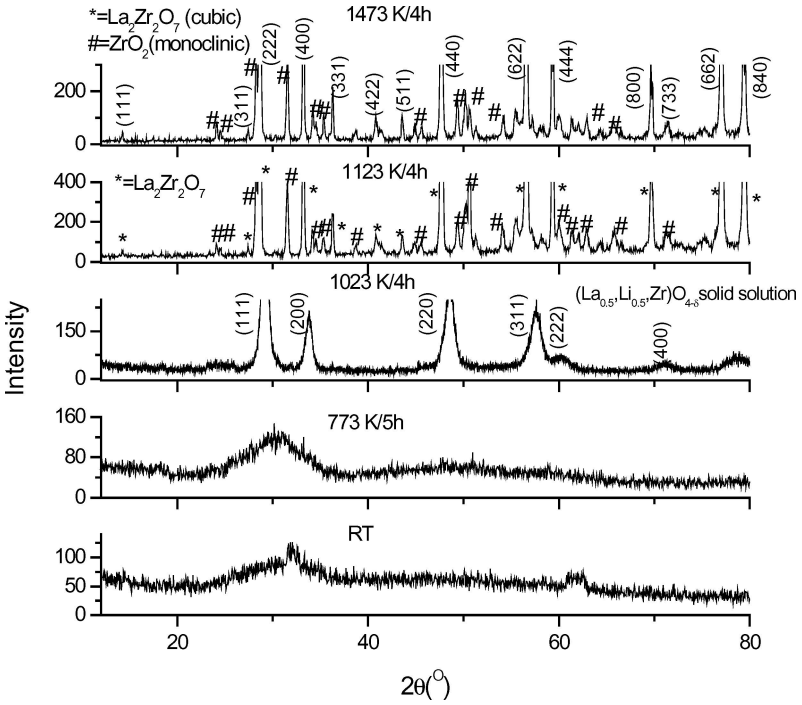

Figure 7 XRD patterns of $(La_{0.5}Li_{0.5}Zr)O_{2-\delta}$ annealed at indicated temperatures, cubic zirconia is stable below 1023 K, $La_2Zr_2O_7$ (cubic) + ZrO_2 (monoclinic) is observed above 1023 K.

oxygen) in the space group P4/mmm [28], analogous to the superstructure data reported for $La_{2/3}TiO_{3-\delta}$ (δ = 0.007–0.079) [29]. In contrast, orthorhombic perovskite [16–18, 30] or tetragonal tungsten bronze structures were reported for compounds prepared by solid state reaction routes or annealed at temperatures above 1673 K for long durations. The sintering of the powders at 1673 K may cause loss of Li^+ and create more vacancies and hence the change in structure.

3.2. Phase behaviour of $(La_{0.5}Li_{0.5})MO_3$ (M = Ce,Zr) compositions

The compositions $La_{1-x}Li_xMO_3$ (M = Zr and Ce, x = 0.5) did not stabilize in perovskite structutre. The XRD patterns of these compositions are given in Figs 6 and 7. The lattice parametrs of the compositions are given in Table I. The experimentally measured lattice parameters were compared with the literature data [31]. The space group and atomic-coordinates

of the ideal structures of these compositions are taken from FIZ/NIST Inorganic Crystal Structure Database (ICSD) [31]. The replacement of Ti with Zr or Ce did not form perovskite phases. The Ce substituted composition formed $((La_{0.5}Li_{0.5})_2Ce)O_4$ solid solution and did not form any other phase on annealing upto 1673 K (Fig. 6). The ionic radii of Ce^{4+} (8-coordinated) in CeO_2 is 1.11 Å (i.e. $r^{VIII}_{Ce^{4+}} = 1.11$ Å), $r^{VIII}_{La^{3+}} = 1.30$ Å, $r^{VIII}_{Li^+}$, = 1.06 Å and $r^{VIII}_{O^{2-}} = 1.40$ Å [32]. The XRD patterns were indexed to cubic CeO_2 (S.G = Fm3m) with expanded lattice constant. The lattice constant for CeO_2 ($a = 5.412$ Å) and for the solid solution is $a > 5.412$ Å are given in Table I. The expansion of lattice is attributed to the accommodation of bigger size ion compared to Ce^{4+} ionic radii.

The Zr substituted compositions form solid solutions of $((La_{0.5}Li_{0.5})_2Zr)O_4$ below 1023 K. The XRD patterns of $((La_{0.5}Li_{0.5})_2Zr)O_4$ are shown in Fig. 7. The lattice constants obtained on indexing the patterns show expansion of parent ZrO_2 lattice. The expansion in lattice constant is attributed to the accommodation of La^{3+} and Li^+ ions in Zr-sublattice. The ionic radii of La^{3+} (i.e. $r^{VIII}_{La^{3+}} = 1.30$ Å) and Li^+ ($r^{VIII}_{Li^+}$, = 1.06 Å) [31] are marginally higher than that of Zr^{4+} in cubic ZrO_2 (i.e. $r^{VIII}_{Zr^{4+}} = 0.98$ Å) [31]. The cubic structure of ZrO_2 was observed to be stable below 1023 K. However, on annealing above 1100 K, $La_2Zr_2O_7$ (pyrochlore) is formed. The transformation of nano-crystalline zirconia solid solution to $La_2Zr_2O_7$ and minor monoclinic ZrO_2 phases are shown in Fig. 7.

3.3. Effect of temperature on electrical transport

Since $La_{0.5}Li_{0.5}TiO_3$ (LLTO) could be prepared as single-phase material by various wet chemical methods, electrical conductivity measurements were carried out on these. The materials prepared by wet chemical routes and sintered at 1473–1523 K show measurable electrical conductivity at 298 K by ac as well as dc techniques. The electrical conductivity (at 298–570 K)

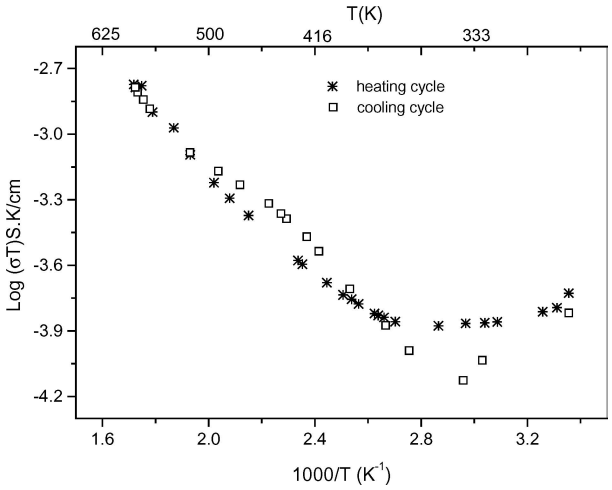

Figure 8 Log (σT) vs. $1/T$ plots of $La_{0.5}Li_{0.5}TiO_3$ (at 298–570 K) prepared by PVA gel decomposition and subsequent annealing at 1523 K /4 h (tetragonal structure).

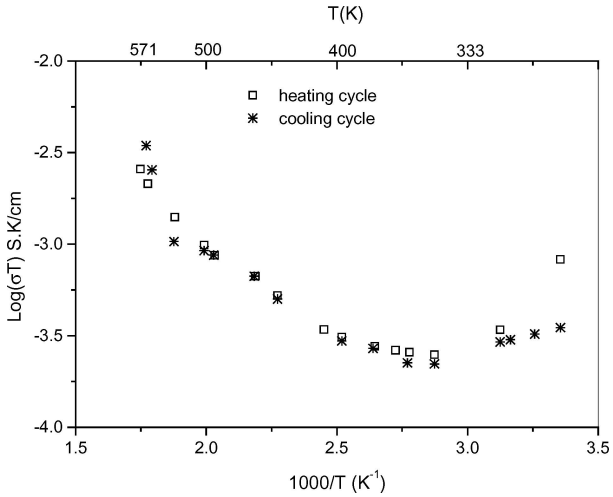

Figure 9 Log (σT) vs. $1/T$ plots of $La_{0.5}Li_{0.5}TiO_3$ (at 298–570 K) prepared by hydro-thermally processed TiO_2 and $La(OH)_3$ gel + $LiOH.H_2O$ and subsequent annealing at 1473 K /4 h.

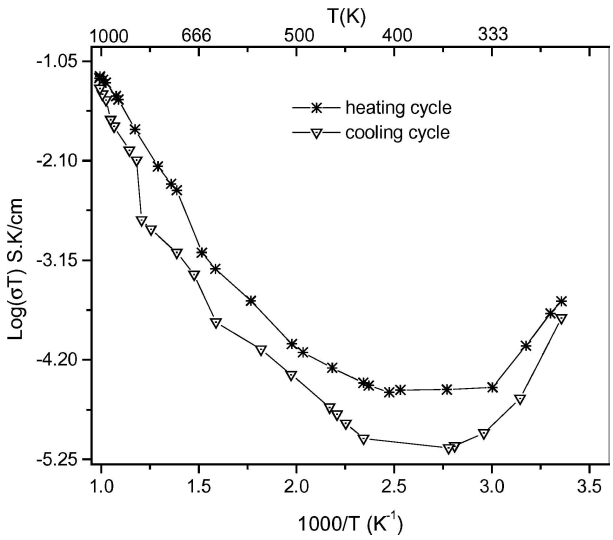

Figure 10 Log (σT) vs. $1/T$ plots of $La_{0.5}Li_{0.5}TiO_3$ (at 298–1000 K) prepared by PVA gel decomposition and subsequent annealing at 1273 K /4 h (after acetic acid leaching under hydrothermal conditions).

of LLTO prepared by (i) PVA gel decomposition and (ii) hydrothermally processed TiO_2 precursor is given in Figs 8–9. The electrical conductivity of LLTO pellet (prepared by PVA gel decomposition) annealed at 1273 K for 4 h then subjected to leaching in acetic acid medium under hydrothermal conditions is given in Fig. 10. The conductivity of these compositions show a decreasing trend below 375–390 K for the first cycle of measurement (heating cycle) indicating the contribution of surface adsorbed H_2O on the specimen. The contribution of hydroxyls towards electrical conductivity is negligible for the materials heated at or above 1473 K. The absence of hydroxyls was confirmed from the IR examination of the samples sintered at 1473 K (Fig. 4). The LLTO sample sintered at 1273 K (hydrothermal leaching not done) also did not contain hydroxyl groups in the lattice. Samples sintered at 1473 K and hydrothermally treated in 1:1 = D_2O:H_2O medium did not show IR absorption peaks corresponding to O─D nor O-H stretch indicating non-incorporation of hydroxyls into the LLTO lattice at neutral pH. Hence,

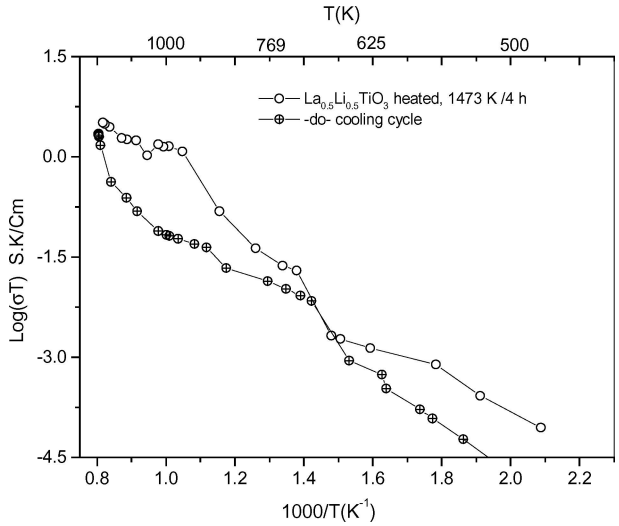

Figure 11 Log (σT) vs. $1/T$ plots of $La_{0.5}Li_{0.5}TiO_3$ prepared by hydrothermally processed TiO_2 and $La(OH)_3$ gel + $LiOH.H_2O$ and subsequent annealing at 1473 K /4 h.

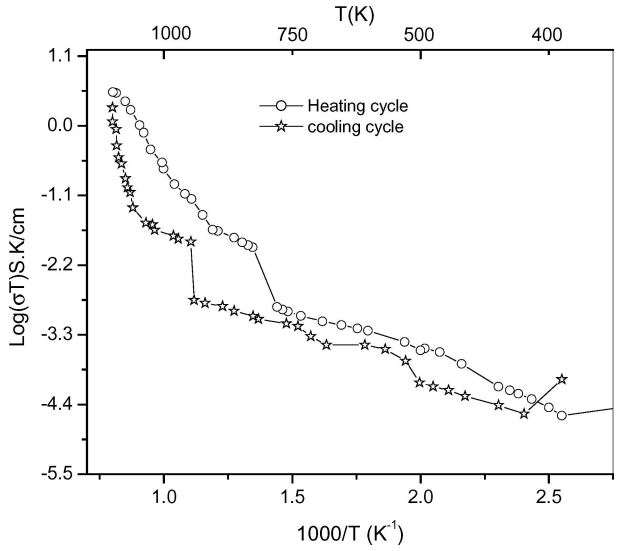

Figure 12 Log σT vs. $1/T$ plot of $La_{0.5}Li_{0.5}TiO_3$ prepared by PVA gel decomposition route and sintered at 1473 K/4 h, tetragonal structure (no leaching carried out on this composition).

the electrical transport in LLTO perovskites (heated at 1473 K) may be due to the mobility of Li^+ ions in the lattice. Most of the investigators believe the LLTO structure supports the migration of Li^+ ions via vacancies available on A-sites [6, 33–35]. However, the samples treated under hydrothermal conditions in acetic acid (10% v/v) medium contain hydroxyl groups in the lattice (Fig. 4). The electrical conductivity of this composition is higher than that of the unleached compositions at 298–400 K. This may be attributed to the presence of hydroxyls in the lattice. The overall conductivity of this composition is less compared to the unleached compositions (Figs 11–13). This may be due to the loss of Li^+-ion (current carriers) due to leaching in acetic acid medium under the hydrothermal conditions.

The electrical conductivity of the samples having cubic crystal structure shows slightly higher conductivity value compared to tetragonal structure. The log (σT) vs. $1/T$ plots are given in Figs 8–10. However, the conductivity values of the three pellets can not be compared, because these were prepared by using different methods. The preparation methods have influences on crystal structure stabilization. Cubic crystal structure is stabilized by using hydrothermal precursor method of preparation and annealing the powders at and below 1273 K. The log (σT) values shown in Fig. 8 at $T = 500$ K or $1000/T = 2$ is about -3.2 S.K/cm and the value shown in Fig. 9 at the same temperature is ~ -2.8 S.K/cm. This clearly shows that cubic LLTO has slightly higher conductivity value. The lower conductivity in tetragonal phases may be attributed to the unequal ordering of Li, La and vacancies along the c-axis. The log (σT) value given in Fig. 10 is about -4.2 S.K/cm at $T = 500$ K is attributed to the leaching out of Li^+. The results given in Figs 8–10 reveal that conductivities of the specimens vary with process conditions. In all the conductivity measurements, log (σT) vs. $1/T$ did not show continuous straight line at 298–1273 K. A break/ bend in the conductivity curve occurred at 550–588 K. This may be attributed to the phase transition in the material or participation of other current carriers above 550 K, thus giving rise to a conduction process with two different activation energies. Similar behaviour for LLTO was reported by several investigators [8–12]. Most of the authors describe the conduction behavior of LLTO as thermally activated process as observed in ionic conducting glasses [36] and define such dependence as non-Arrhenius behaviour [37–39].

The AC impedance studies on the specimens were carried out at 298–900 K with Pt electrodes. The semicircle at the low frequency end of the impedance plot indicates blocking effect of Pt electrode to the mobility of Li^+ ions. The bulk conductivity was observed at high frequency end of the impedance plot. The effect of temperature on the conductivity of the specimen was evident from the decrease of impedance as shown in Figs 14–19. The impedance of the specimens decreases on increasing the temperature of measurement, indicating increase in conductivity of the pellet. This may be attributred to the thermally activated mobility of the ions. The time constant $(\tau = RC)$ of the diffusion process was evaluated using formula $\omega_p RC = 1$, i.e $\tau = 1/\omega_p$, where ω_p is the peak frequency of the semi-circle, R is the resistance and C is the capacitance of the equivalent circuit [40, 41]. The time constant value of the semi-circle corresponding to bulk conductivity is of the order of 10^{-3} to 10^{-4} s. The composition leached in dilute acetic acid medium under hydrothermal condition shows higher impedance (low conductivity) compared to unleached compositions (e.g., impedance for unleached composition at $\sim$500 K in Fig. 14 is lower $(6 \times 10^5 \Omega)$ than that for leached composition $(7.5 \times 10^6 \Omega)$ in Fig. 16 at $\sim$ 500 K). This trend was also observed in dc conductivity meausrements. The loss of Li^+ under leaching condition is ascribed to this observation. The effect of annealing temperature on the electrical conductivity of the pellets was clearly seen in ac impedance measurements. The samples sintered at 1173 as well as 1273 K show two semicircles in the impedance plot (Figs 14–17),

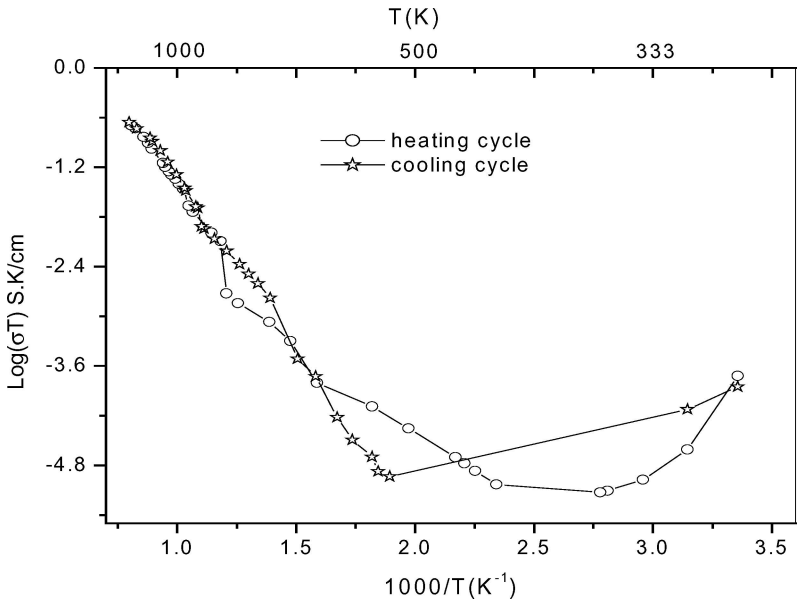

Figure 13 Log (σT) vs. $1/T$ plots of $La_{0.5}Li_{0.5}TiO_3$ (at 298–1000 K) prepared by PVA gel decomposition and subsequent annealing at 1273 K /4 h (after acetic acid leaching under hydrothermal conditions).

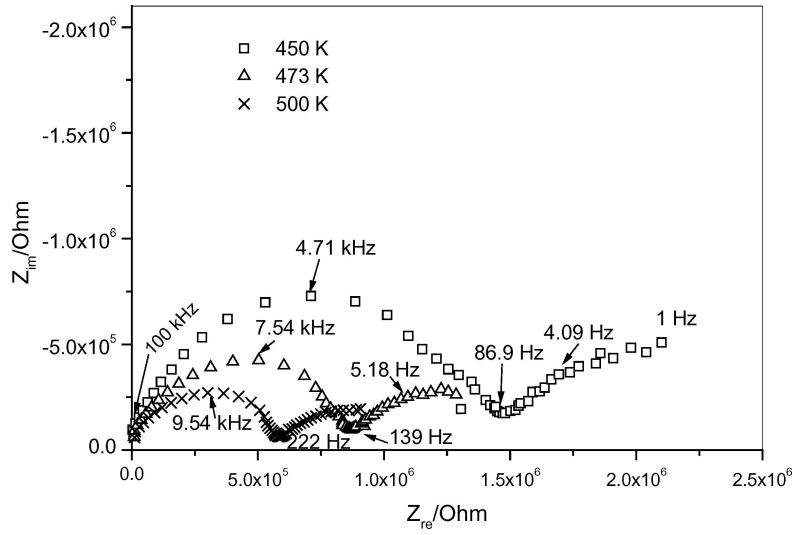

Figure 14 Impedance plot of $La_{0.5}Li_{0.5}TiO_3$ prepared by PVA gel decomposition heated at 1173 K (no leach treatment).

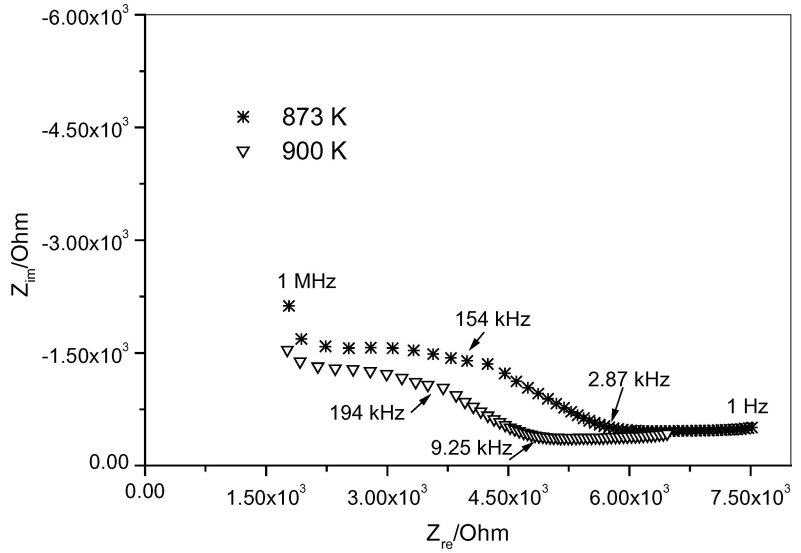

Figure 15 Impedance plot of $La_{0.5}Li_{0.5}TiO_3$ prepared by PVA gel decomposition heated at 1173 K (no leach treatment).

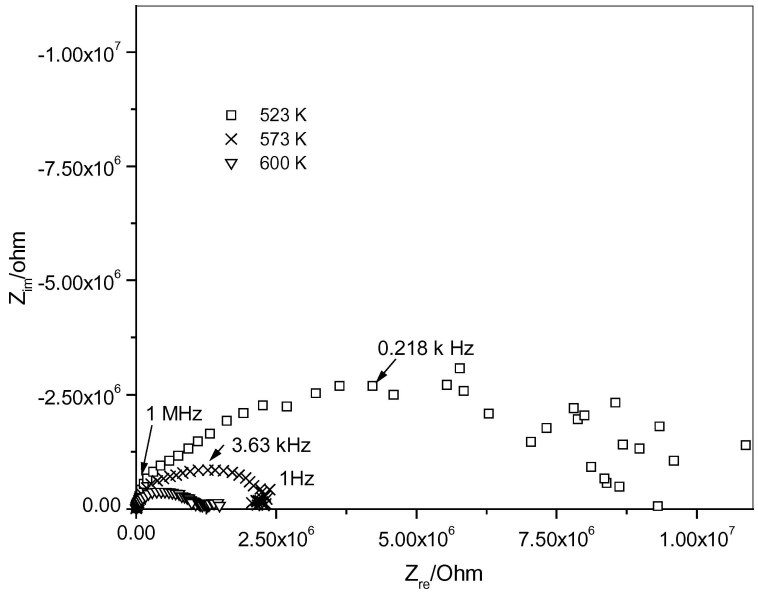

Figure 16 Impedance plot of $La_{0.5}Li_{0.5}TiO_3$ prepared by PVA gel decomposition route heated at 1273 K, hydrothermal treatment of the pellet in acetic acid medium at 423 K/5 h before impedance measurement carried out on the pellet at indicated temperatures.

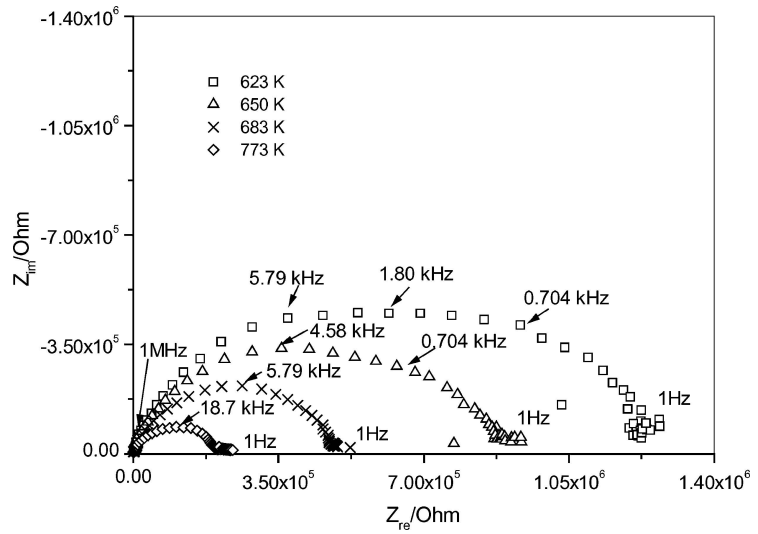

Figure 17 Impedance plot of $La_{0.5}Li_{0.5}TiO_3$ prepared by PVA gel decomposition route heated at 1273 K, measurement carried out at indicated temperatures after hydrothermal treatment of the pellet in acetic acid medium.

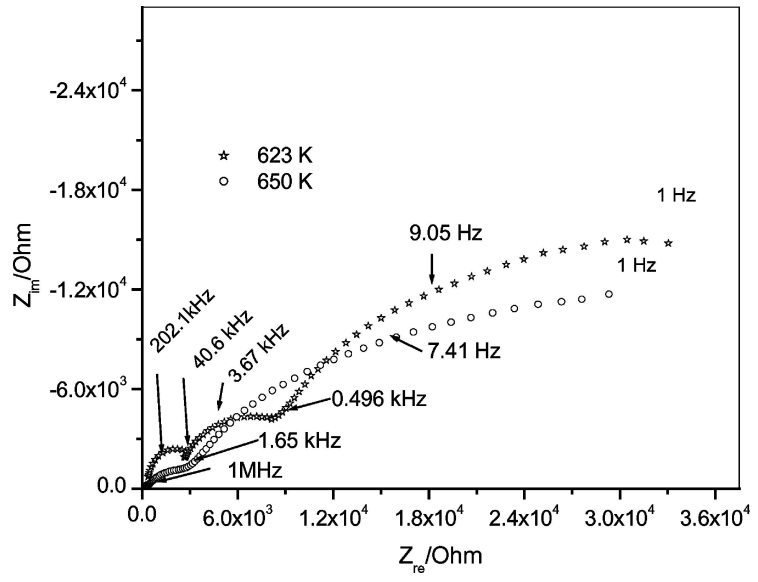

Figure 18 Impedance plot of $La_{0.5}Li_{0.5}TiO_3$ pellet treated under hydrothermal condition at 423 K (pellet originally sintered at 1523 K/4 h) and measurement carried out at indicated temperatures.

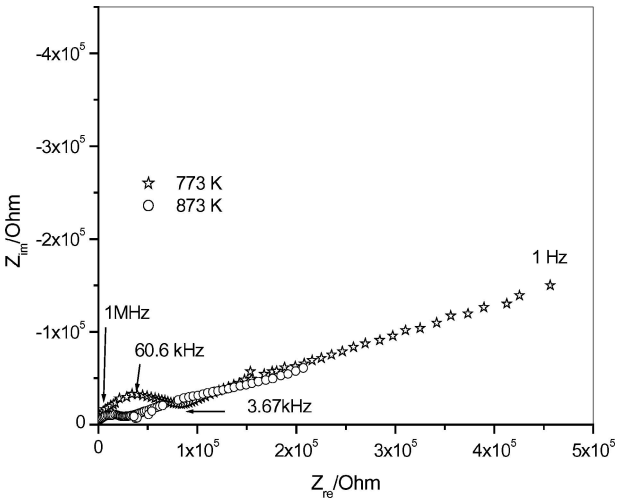

Figure 19 Impedance plot of $La_{0.5}Li_{0.5}TiO_3$ pellet treated under hydrothermal condition at 423 K(pellet originally sintered at 1523 K/4 h) and measurement carried out at indicated temperatures.

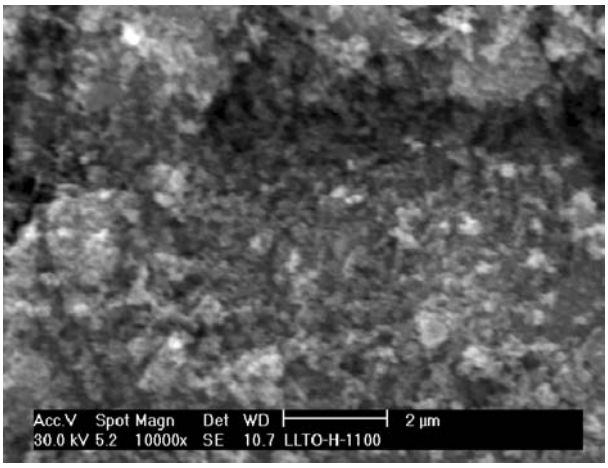

Figure 20 SEM micrograph of $La_{0.5}Li_{0.5}TO_3$ green pellet prepared from hydrothermal precursors, heat-treated at 1073–1100 K/4 h.

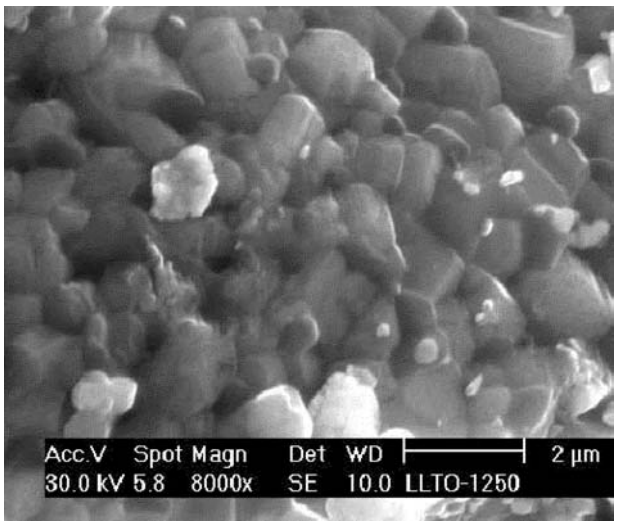

Figure 21 SEM micrograph of $La_{0.5}Li_{0.5}TO_3$ pellet sintered at 1523 K/4 h.

whereas samples sintered at 1523 K shows 3 semicircles in impedance plot measured at 623 K (Figs 18 and 19). This may be attributed to the formation of distinct grain as well as grain boundaries on sintering the pellets at 1523 K. The grain and grain boundaries are shown in SEM micrograph (Fig. 21). The SEM micrograph of pellets sintered at various temperatures is shown in Figs 20 and 21. The powders heat-treated at 1100 K and pressed to pellet (green pellet without sintering) shows particles of 180–200 nm size (Fig. 20). On sintering the pellets to higher temperatures the particles grew to 1–2 μm size (Fig. 21). The particles with this size showed 2–3 semicircles in the impedance plot at 500–700 K. The semicircle at low frequency end of the plot (Fig. 18) corresponds to the electrode polarization process; the semi-circle at 0.496–40.6 kHz (middle one) corresponds to grain boundary (intergrain) impedance and the semi-circle at high frequency end of the plot correspond to intra grain impedance of the sample. On increasing temperature the impedance due to intragrain for the current flow became negligible and the semicircle did not appear in the impedance plot as shown in Fig. 18 for 650 K and Fig. 19 at 773 and 873 K. Similarly for samples sintered at 1173 or 1273 K, the intragrain impedance vanishes on increasing the temperature.

Several conduction mechanisms have been proposed for LLTO based on structural considerations, concentration of vacancy, bottleneck for Li^+ migration and tilting of TiO_6 octahedra. The high ionic conductivity is believed to be due to the migration of Li^+ ions. The ionic conductivity ($\sigma = nZ_e\mu$) depends on the carrier (i.e Li^+ with $Z_e = 1$) concentration (n) and mobility (μ) of the ions. The mobility mainly depends on the activation energy of the ionic conduction and the bottleneck size [8, 33, 35] of the Li^+ ion-conducting channel. The ionic conduction was evidenced from the hysterysis obtained on heating and cooling cycle measurements (Figs 11–13). The hysterysis may be attributed to the polarization of the electrodes because of blocking character of Pt- electrodes towards Li^+.

4. Conclusion

The structure and electrical conductivity of $Li_{3x}La_{(2/3)-x}V_{(1/3)-2x}TiO_3$ composition depend on the preparation condition of the material. The carrier concentrations can be improved by adopting wet-chemical routes. The wet chemical preparation can produce cubic crystal structure and thus provide better structural framework for the enhanced mobility of Li^+ ions. Compositions having cubic crystal structure show higher conductivity than tetragonal structure. The samples sintered at 1523 K show distinct semicircles in the impedance pattern indicating better crystallinity of the material in contrast to the pellets sintered at 1173–1273 K. The samples prepared by hydrothermally treated precursor process or hydroxyls incorporated by hydrothermal treatment show higher conductivity below 400 K. The samples prepared by PVA gel decomposition or carbonate route do not show presence of hydroxyls in the lattice. The conductivity in this case arises due to Li^+ mobility. The decrease of conductivity on leaching out Li^+ from the lattice by hydrothermal treatment in acetic acid medium confirms the vital contribution of Li^+ concentration towards ionic conductivity in $La_{0.5}Li_{0.5}TiO_3$. The contribution of hydroxyls if present may be negligible

towards electrical conduction above 550 K .The 100% substitution of Ce at Ti sublattice does not form perovskite phase, rather it forms $(La_{0.5}Li_{0.5})_2CeO_4$ solid solution below 1673 K. The 100% substitution of Zr at Ti site forms solid solution below 1073 K and above this temperature $La_2Zr_2O_7$ along with minor phase of monoclinic zirconia are formed.

References

1. A. KVIST and A.LUNDEN, *Z. Naturforsch* **20a** (1965) 235.
2. A. R. WEST, *J. Appl. Electrochem.* **3** (1973) 327.
3. P. G. BRUCE and A. R. WEST, *Mater. Res. Bull.* **15** (1980) 117.
4. H. AONO, E. SUGIMOTO, Y. SADAOKA, N. IMANAKA and G. ADACHI, *J. Electrochem. Soc.* **136** (1989) L590.
5. L. LATIE, G. VILLENEUVE, D. CONTE and G. L. FLEM, *J. Solid State Chem.* **51** (1984) 293.
6. M. OGUNI, Y. INAGUMA, M. IOTH and T. NAKAMURA , *Solid State Commun.* **91** (1994) 627.
7. A. G. BELOUS, G. N. NOVITKAYA, S. V. POLYANETSKAYA and Y. I. GORINKOV, *Izv. Akad. Nauk. SSSR, Neorg. Mater.* **23** (1987) 470.
8. Y. INAGUMA C. LIQUAN, M. ITOH and T. NAKAMURA, *Solid State Commun.* **86** (1993) 689.
9. H. KAWAI and J. KUWANO, *J. Electrochem. Soc.* **141** (1994) L78.
10. Y. INAGUMA C. LIQUAN, M. ITOH and T. NAKAMURA, *Solid State Ionics* **70/71** (1994) 196.
11. Y. INAGUMA and M. ITOH, *ibid.* **86–88** (1996) 257.
12. S. STRAMARE, V. THANGADURAI and W. WEPPNER, *Chem. Mater.* **15** (2003) 3974.
13. S. KUNUGI, Y INAGUMA and M. ITOH, *Solid State Ionics* **122** (1999) 35.
14. J. BROUS, I. FANKUCHEN and E. BANKS, *Acta Crystallogr.* **6**(1) (1953) 67.
15. P. V. PATIL and V. C. CHINCHOLKAR, *Curr. Sci.* **39**(2) (1970) 348.
16. *Idem.*, *Indian J. Chem. Sect.* **A 16**(2) (1978) 161.
17. A. M.VARAPRASAD, A. L. S.MOHAN, D. K. CHAKRAVARTY and A. B. BISWAS, *J. Phys. C. Solid State Phys.***12**(2) (1979) 465.
18. J. L. FOURQUET, H. DUROY and M. P. C. LOPEZ, *J. Solid State Chem.* **127** (1996) 283.
19. C. A. KIRK and A. R. WEST, *Solid State Sci.* **4** (2002) 1163.
20. A. M ORRANTIA, S. G. MARTIN and M. A. A. FRANCO, *Chem. Mater.* **15** (2003) 363.
21. A. D. ROBERTSON, S. G. MARTIN, A. COATS and A. R. WEST, *J. Mater. Chem.* **5**(9) (1995) 1405.
22. K. KITAOKA, H. KOZUKA, T. HASIMOTO and T. YOKO , *J. Mater. Sci.* **32**(8) (1997) 2063.
23. T. R. N.KUTTY and P. PADMINI, *Mater. Res. Bull.* **27** (1992) 945.
24. H. JENA, K. V. G. KUTTY and T. R. N. KUTTY, *ibid.* **39** (2004) 489.
25. H. JENA, K. V. G. KUTTY and T. R. N. KUTTY, *J. Alloys Comp.* **350** (2003) 102.
26. *Idem.*, *Mater. Chem. Phys.* **88** (2004) 167.
27. J. BROUS, I. FANKUNCHEN and E. BANKS, *Acta. Crystall.* **6**(1) (1953) 67.
28. J. L. FOURQUET, H. DUROY and M. P. L-CROSINER, *J.Solid tate Chem.* **127** (1996) 283
29. M. ABE and K. UCHINO, *Mater. Res. Bull.* **9** (1974) 147.
30. L. L. KOCHERGINA , N. B. KHAKHIN, N. V. POROTNIKOV and I. PETROV, *Russ. J. Inorg. Chem.* **29**(4) (1984) 506.
31. FIZ/NIST Inorganic Crystal Structure Database (ICSD) version 1.2.1, Karlsruhe, Germany 2003.
32. R. D. SHANNON , *Acta Crystallogr.* **A32** (1976) 751.
33. M. IOTH, Y. INAGUMA, W. H. JUNG, L. CHEN and T. NAKAMURA, *Solid State Ionics* **70/71** (1994) 203.
34. Y. INAGUMA, J. YU, Y. J. SHAN, M. IOTH and T. NAKAMURA, *J. Electrochem. Soc.* **142** (1995) L8.
35. V. THANGADURAI, A. K. SHUKLA and J. GOPALAKRISHNAN, *Chem. Mater.* **11** (1999) 835.
36. J. KINCS and W. S. MARTIN, *Phys. Rev. Lett.* **76** (1996) 70.
37. C. LEÓN, M. L. LUCÍA, J. SANTAMARÍA, M.A PARIS, J.SANZ and A. VÁREZ, *Phys. Rev.* B **54** (1996) 184.
38. K. M. NAIRN, M. FORSYTH, M. GREVILLE, D. R. MACFARLANE and M. E SMITH , *Solid State Ionics* **86–88** (1996) 1397.
39. O. BOHNKE, C. BOHNKE and J. L. FOURQUET, *Solid State Ionics* **91** (1996) 21.
40. K. S. COLE and R. H. COLE, *J. Chem. Phys.* **9** (1941) 341.
41. J. R. MACDONALD, IN "Impedance Spectroscopy, Emphasizing Solid Materials and Systems" (Wiley Inter-Science, New York, 1987) p. 6.

Received 16 October 2004
and accepted 14 February 2005